

EPR and electron-nuclear double-resonance studies of an F^+ center in sodium, potassium, and lithium β -alumina

S. R. Kurtz,* D. G. Stinson, and H. J. Stapleton

Department of Physics and Materials Research Laboratory, University of Illinois at Urbana-Champaign, Urbana, Illinois 61801

M. M. Abraham

Solid State Division, Oak Ridge National Laboratory, Oak Ridge, Tennessee 37830

(Received 13 July 1981)

EPR and electron-nuclear double-resonance (ENDOR) data from F^+ centers in the conduction planes of sodium, potassium, and lithium β -alumina are presented. The low-temperature Ku-band ENDOR spectra from these fast ionic conductors consist of sharp resonances from distant nuclei and broad, unresolved signals from nearest-neighbor aluminum and nearby Na, K, or Li cations in the conduction plane. The Na data are consistent with x-band ENDOR results of others. The K and Li data reveal the existence of a second inequivalent F^+ center in these materials. The shape and breadth of the Na ENDOR signal can be simulated assuming that: (1) both Beavers-Ross and mid-oxygen sites are occupied, (2) the F^+ -ligand hyperfine interaction varies with distance as $1/R^3$, and (3) there exists a Gaussian distribution of hyperfine couplings which is consistent with a 0.3-Å tunneling distance inferred for Na ions from dielectric susceptibility data on Na β -alumina.

I. INTRODUCTION

β -alumina is a family of materials which exhibits fast ionic conduction at high temperatures. In addition thermal conductivity,¹ specific heat,² and dielectric susceptibility data^{3,4} at low temperatures have established that these materials display glasslike behavior near 1 K. Both the high ionic conductivity and the low-temperature glasslike properties of β -alumina are the result of the intrinsic disorder in the mirror planes of the structure, which is shown for the sodium salt in Figs. 1 and 2. The disorder in the conduction plane is due to a 15–30% stoichiometric excess concentration of the mobile cation.⁵ Paramagnetic centers can be formed in the conduction planes by irradiation. An F^+ center, associated with a trapped electron at an oxygen vacancy in the conduction plane, is shown schematically in Fig. 3. These, and other centers, have been independently observed and reported by several investigators.^{6–8} In earlier papers we have reported how the disorder in the conduction plane of β -alumina influences the electron-spin relaxation of an F^+ center, and leads to an anomalous temperature dependence of the relaxation rate.^{7,9,10} Our quantitative calculations in

those papers relied in part upon electron-nuclear double-resonance (ENDOR) data which we now report along with a more complete analysis of the EPR spectra. Experimental data and its interpretation are presented for each of the three systems studied. This is followed by a more complete discussion of those features which appear common to all three systems. Evidence indicating the existence of two inequivalent F^+ centers within the conduction planes of K and Li β -alumina will be presented.

II. EXPERIMENTAL DETAILS

All the samples used in these measurements were loaned to us by A. C. Anderson and P. J. Anthony who used them in their specific-heat, thermal conductivity, and dielectric susceptibility measurements.^{1–3} Single crystals of Na β -alumina were obtained from Union Carbide and converted, as needed, to the Li and K salts by repeated ion exchange.¹¹ All samples were stored in an anhydrous environment, and as a further precaution the Li β -alumina was dehydrated before irradiation by heating to 300 °C for 48 h in a vacuum.

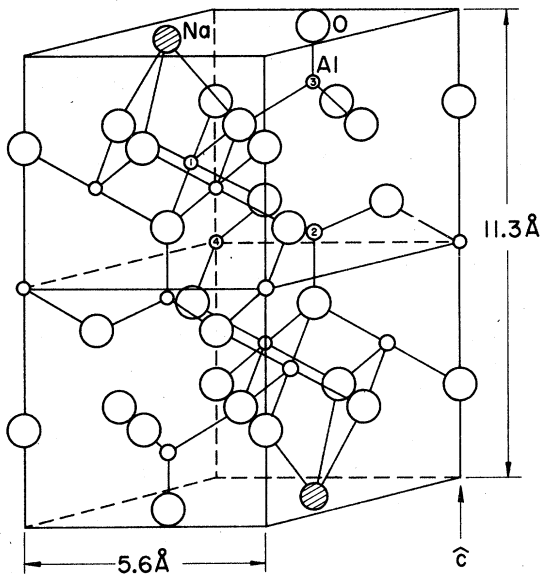


FIG. 1. Stoichiometric structure of Na β -alumina. Half of a unit cell is shown and the Na cations occupy BR sites. The Na ions are located in conduction planes perpendicular to the \hat{c} axis. The four different Al atoms are labeled within the figure (Ref. 32).

In order to study β -alumina with EPR techniques, it is necessary to introduce paramagnetic centers into the conduction plane. This can be accomplished by substituting transition metal ions for Na ions¹²⁻¹⁴ or by irradiating the material to pro-

duce color centers. We have used the latter approach, employing primarily electron irradiation at liquid-nitrogen temperatures. Some of our experiments were performed on γ -irradiated samples. Other research groups have produced color centers in β -alumina with uv, x-ray, or γ -ray irradiation.^{6,8}

During sample exposures to 1.5-MeV electrons from a Van de Graaff accelerator, a 50- μ m thick Ti foil was placed between the incident electron beam and the sample. This foil scattered the electrons and produced bremsstrahlung x rays. Without this foil, the efficiency of the color-center production was greatly decreased. Exposures were typically 5 min with a dosage of between 10^{13} and 10^{14} electrons.

When the irradiated samples were kept at low temperatures, they exhibited a dark blue coloration and displayed EPR spectra corresponding to the F^+ center and another unidentified center. The blue coloration and interfering EPR signal could be destroyed by warming the Na or Li samples to room temperature. After this annealing, the samples had a slightly yellow-brown tint which together with the F^+ EPR signal persisted indefinitely if kept at 77 K. However, in K β -alumina both paramagnetic centers bleached at roughly the same rate. When Na β -alumina was irradiated with 0.75-MeV electrons at low temperature, no F^+ center was produced. The blue coloration and the unidentified paramagnetic center were generated

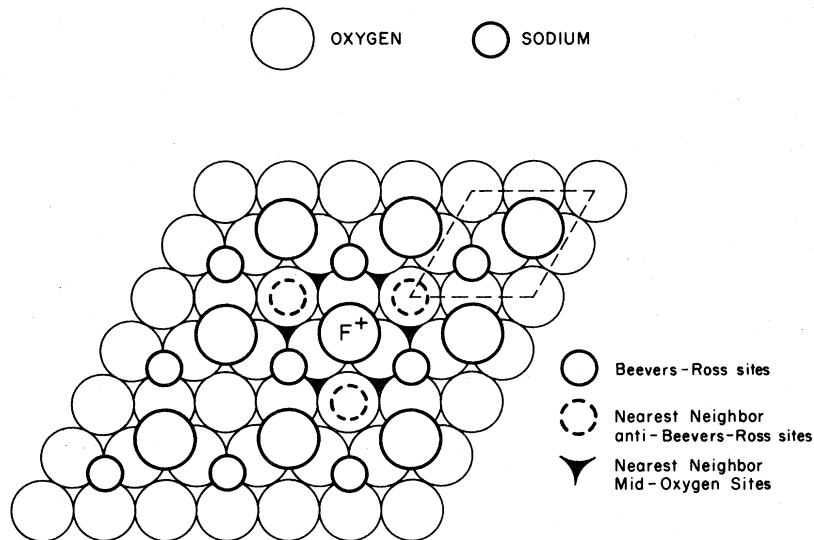


FIG. 2. Structure of the conduction plane of stoichiometric Na β -alumina. The location of the F^+ center and the nearby BR, MO, and aBR sites are shown. Light circles are the close-packed oxygen layer above and below the conduction plane. The unit cell of Fig. 1 is indicated by the dotted line.

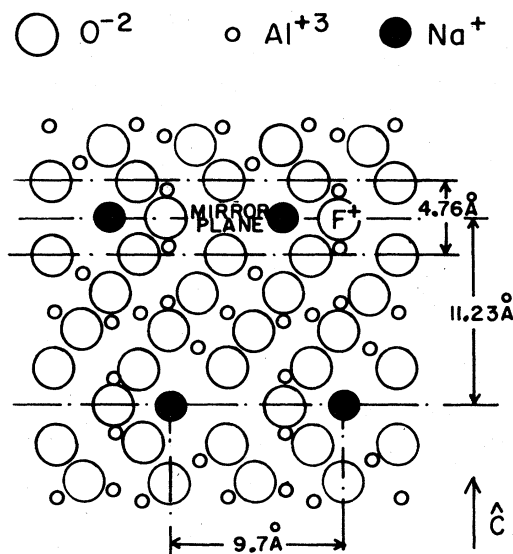


FIG. 3. Structure of stoichiometric Na β -alumina with the probable position of an F^+ center indicated within the conduction plane at a bridge oxygen site. Above and below the F^+ center are the two equivalent Al nuclei which produce the observed hyperfine lines in the EPR spectrum. A Na^+ cation BR site is located 3.2 Å from the F^+ center.

under these conditions, but vanished rapidly at room temperature. The F^+ center in Na or Li β -alumina could be destroyed by heating the samples in vacuum at 200 °C.

The unidentified center could also be produced by γ irradiation at 77 K using a ^{137}Cs source. The resulting EPR spectrum for Na β -alumina exhibited axial symmetry about the crystallographic \hat{c} axis. With the external magnetic field parallel to the \hat{c} axis, the EPR absorption line at 9.1 GHz was a broad (43-G peak-to-peak derivative linewidth), symmetric, and structureless signal centered at $g_{\parallel} = 2.048(5)$. When the field was perpendicular to the \hat{c} axis, some structure appeared superimposed on the broad resonance (50-G peak-to-peak derivative) in the form of 10 to 12 sharp, equally spaced hyperfine (hf) lines of unequal intensity. These were centered at $g_{\perp} = 2.002(9)$ and separated by approximately 7.5 G. Isochronal annealing measurements between 117 K and room temperature, using 6-min heating periods, indicate that this center is stable to about 225 K. These measurements also indicate that the F^+ center is not directly generated by the low-temperature γ irradiation. Rather, it appears to form as one of the decay products of the unidentified center. Signals from both centers

could be seen after isochronal annealing, with most of the F^+ production occurring in the 0 to +5 °C temperature range. The sum of the precursor and the F^+ EPR signals did not, however, remain constant. A room temperature γ irradiation of Na β -alumina produced the F^+ center directly.

The EPR results we report here were obtained primarily from a homebuilt x-band homodyne spectrometer which used 40-kHz magnetic-field modulation and a cylindrical TE_{011} mode cavity which resonated near 9.3 GHz. A quartz tube, 10 mm o.d. \times 1 mm wall, within and coaxial to the cavity, permitted easy sample rotation and sample exchange. In addition, the sample could be cooled by cold nitrogen gas which flowed through the tube. A maximum magnetic field modulation of 4 G (peak-to-peak) was generated by running alternating current through two brass rods, 1.6 mm in diameter, parallel to the sample tube, and electrically connected as a one-turn coil.

All ENDOR measurements reported here were done below the λ point of liquid helium using a cylindrical TE_{011} mode cavity which resonated near 15.0 GHz. The rf coil was constructed by encapsulating three strands of Formvar-coated 32-gauge copper wire inside a thin-walled, 0.9-mm-o.d., copper tube with Stycast 1266 epoxy.¹⁵ The copper tube was stripped from a 0.9-mm-o.d. Coax-itube.¹⁶ Two of these modulation rods were placed in the cavity parallel to the cavity axis with the wires soldered together to form a 3-turn rf coil. Coils constructed in this manner operated well over a 3–40-MHz frequency range and were resistant to vibration and thermal stress. The resultant ENDOR cavity had a Q of approximately 8000 and the intensity of the rf field at the sample was an order of magnitude larger than that achieved with a slotted cavity-coil design having a comparable bandwidth.¹⁷

An LSI-11 microcomputer controlled the frequency sweep of the rf coil and also functioned as an ENDOR signal averager. The microwave absorption signal from a Ku-band superheterodyne spectrometer was collected during the up and the down sweeps of the rf signal generator. This procedure eliminated ENDOR lineshape distortion which is occasionally present with unidirectional frequency sweeps. The microcomputer controlled the rf frequency through a digital-to-analog converter, and digitized and stored the absorption signal. After signal averaging was completed, the frequency of each step in the resulting ENDOR spectrum was measured using a frequency counter con-

nected to the LSI-11 via an IEEE-488 Bus. The data were then transferred to a floppy disk for further analyses.

III. COLOR CENTER SPIN HAMILTONIAN

The spin Hamiltonian for a spin- $\frac{1}{2}$ color center with ligand-hf interactions is

$$\mathcal{H} = \mu_B \vec{S} \cdot \underline{g} \cdot \vec{H}_0 + \sum_i (\vec{S} \cdot \underline{A}_i \cdot \vec{I}_i - g_{ni} \mu_B \vec{I}_i \cdot \vec{H}_0 + \vec{I}_i \cdot \underline{P} \cdot \vec{I}_i), \quad (1)$$

where the terms on the right correspond to electronic-Zeeman, ligand-hf, nuclear-Zeeman, and nuclear-quadrupole interactions, respectively, and i is the index of the ligand nucleus. One of the two contributions to the tensor \underline{A}_i is that associated with an isotropic contact term of the form $a_i \vec{I}_i \cdot \vec{S}$ with

$$a_i = \frac{8}{3} \pi g_e g_{ni} \mu_B^2 |\psi(0)|_i^2, \quad (2)$$

where g_e is the free-electron g value, g_{ni} is the nuclear g factor of the i th ligand expressed in units of the Bohr magneton, and $|\psi(0)|_i^2$ is the electron density of the unpaired spin at the ligand nucleus. The other contribution to \underline{A}_i comes from the electron-nuclear dipole-dipole interaction which adds traceless elements to \underline{A}_i having axial symmetry about the color-center—ligand bond axis. The total result is an axially symmetric \underline{A}_i tensor with principal values: $(a_i - b_i)$, $(a_i - b_i)$, and $(a_i + 2b_i)$.

If only one ligand nucleus is considered, and \underline{g} and \underline{A} are nearly isotropic, but share a common axis of axial symmetry with \underline{P} , then the approximate energy levels which result from Eq. (1) are

$$E(M, m) \approx g \mu_B H_0 M + [a + b(3 \cos^2 \theta - 1)] M m - g_n \mu_B H_0 m + \frac{1}{2} P_{||} [m^2 - I(I+1)/3] \times (3 \cos^2 \theta - 1), \quad (3)$$

where $g^2 = g_{||}^2 \cos^2 \theta + g_{\perp}^2 \sin^2 \theta$, M and m are the electronic- and nuclear-spin components, respectively, and θ is the angle between the applied magnetic field \vec{H}_0 and the axial-symmetry axis. Equation (3) predicts allowed electron-spin transitions ($\Delta M = +1$, $\Delta m = 0$) when

$$h\nu = g \mu_B H_0 + [a + b(3 \cos^2 \theta - 1)] m, \quad (4)$$

where ν is the microwave frequency. For two equivalent ($a_1 = a_2$, $b_1 = b_2$) spin- $\frac{1}{2}$ ligand nuclei,

Eq. (4) predicts 11 equally spaced EPR lines with intensity ratios of 1:2:3:4:5:6:5:4:3:2:1, because of the various combinations of $(m_1 + m_2)$. The ENDOR transitions ($\Delta M = 0$, $\Delta m = \pm 1$) satisfy the relation

$$h\nu_{\text{if}} = | [a + b(3 \cos^2 \theta - 1)] M - g_n \mu_B H_0 + P_{||} (3 \cos^2 \theta - 1)(m \pm 1/2) |. \quad (5)$$

Although these solutions to the spin Hamiltonian appear very specialized, they actually provide a strong foundation for interpreting a wide range of color-center EPR and ENDOR data. As long as \underline{g} and \underline{A} are nearly isotropic, \vec{S} and \vec{I} are quantized in the direction of \vec{H}_0 to a first approximation. Under these conditions, it is possible to modify Eqs. (4) and (5) to handle the case when \underline{g} , \underline{A} , and \underline{P} have differing symmetry axes.^{18,19} Based on this treatment of the spin Hamiltonian, our EPR and ENDOR data are used to evaluate spin-Hamiltonian parameters in Sec. IV.

IV. EPR AND ENDOR OF THE F^+ CENTER

Color centers identified as F^+ centers have been observed in Na, K, and Li β -alumina by EPR and ENDOR techniques.^{6-8,10,20-22} In this section, data on the F^+ center are presented and summarized. For each material, the EPR and ENDOR results are discussed interchangeably because these techniques complement each other, and their data should be consistent. At the end of this section, the arguments leading to the identification of this paramagnetic defect as an F^+ center^{6,8} are reviewed.

A. Na β -alumina results

Irradiation of Na β -alumina with 1.5-MeV electrons, followed by a brief room-temperature annealing, produces a single color center with an EPR spectrum as shown in Fig. 4. The resulting 11-line hf pattern exhibits the intensity ratios characteristic of an electron interacting with two equivalent spin- $\frac{5}{2}$ nuclei, and possesses axial symmetry about the crystallographic \hat{c} axis (perpendicular to the mirror planes). From the angular dependence of the x-band EPR data we determine that $g_{||} = 2.0079(5)$, $g_{\perp} = 2.0039(5)$, $A_{||}/g_{||}\mu_B = (a + 2b)/g_{||}\mu_B = 16.8(2)$ G, and $A_{\perp}/g_{\perp}\mu_B = (a - b)/g_{\perp}\mu_B = 16.3(2)$ G. These results are in good agreement with those obtained by others.^{6,8}

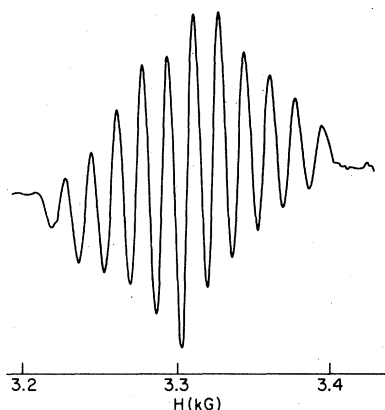


FIG. 4. Derivative of the EPR spectrum of an F^+ center in the conduction plane of Na β -alumina as measured at 77 K and 9.3 GHz, with $\vec{H}_0 \parallel \hat{c}$. A similar EPR spectrum appears in K β -alumina.

The F^+ -center concentration was determined by comparing the intensity of the F^+ EPR signal with the signal produced by a MgO sample doped with a known concentration of Cr^{3+} . This measurement indicated that the irradiation procedure produced $\sim 10^{17} - 10^{18} F^+/cm^3$ in Na β -alumina, and longer irradiations did not visibly increase the color-center concentration. This suggests that the electron irradiation does not generate knock-on lattice defects.

ENDOR spectra of the F^+ center were obtained by saturating the center line of the Ku-band EPR

spectrum at approximately 1.8 K. These spectra revealed several different peaks in the 2–35 MHz range which could be identified as near-Al, near-Na, and distant-Al ligands. Saturation of different hf lines did not significantly change the ENDOR spectra indicating that all of these ENDOR lines belong to the same defect, but saturation of different hf lines did produce slight changes in the ENDOR lineshape, probably due to complex nuclear polarization and relaxation processes. Also, it should be noted that Na, K, and Li β -alumina displayed unusually broad ENDOR lines which limited the amount of information available from the data. This low resolution is probably associated with the disorder in the conduction plane and will be discussed in more detail later.

ENDOR signals were obtained from the two equivalent Al nuclei that produce the resolved hf structure in the EPR spectrum. These are shown in Fig. 5 and appear as two broad peaks centered about A_{\parallel}/h , with a splitting of $2g_{Al}\mu_B H_0/h$. A fit of the angular variation of these ENDOR signals is shown in Fig. 6 and results in values of $a = 45.7(1)$ MHz and $b = 1.0(1)$ MHz, which agree with the EPR values. Each broad Al ENDOR peak consists of five quadrupole peaks with splittings described by a P tensor with axial symmetry along the \hat{c} axis and $P_{\parallel}/h = 0.35(6)$ MHz. Disordered Na^+ ions in the conduction plane should lower the symmetry of the P tensor,²² but we could not resolve such effects.

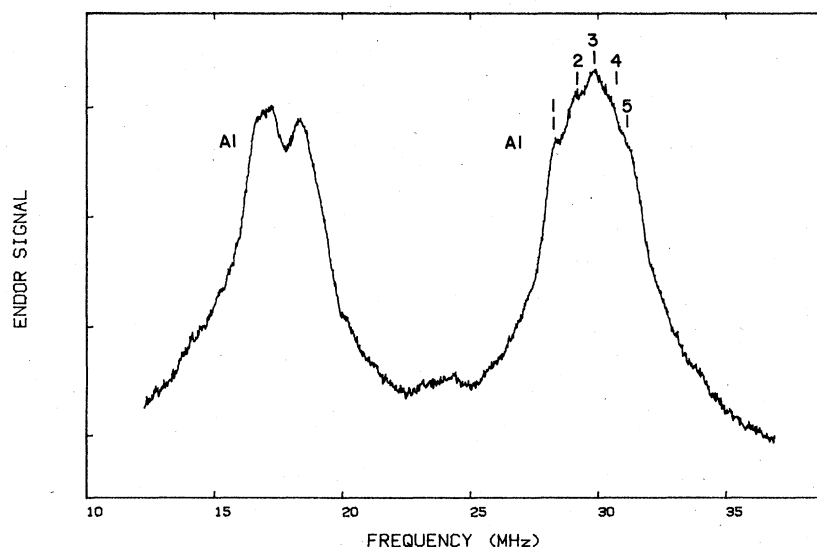


FIG. 5. ENDOR spectrum of near Al nuclei in Na β -alumina. $H_0 = 5346$ G, $\nu = 15.02$ GHz, and $\vec{H}_0 \parallel \hat{c}$. The five-line quadrupolar structure is indicated for one of the peaks.

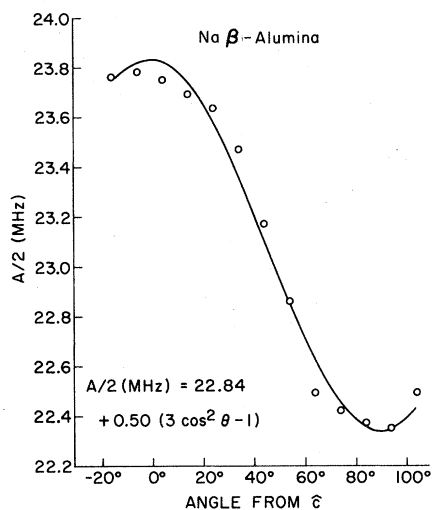


FIG. 6. ENDOR data for the F^+ -Al hyperfine interaction in Na β -alumina as a function of the direction of the applied magnetic field. The solid line is a fit to an A with the form of Eq. (5) of the text.

Figure 7 shows an ENDOR spectrum for Na β -alumina in the 3–13 MHz range, with H_0 set at 5346 G parallel to the crystalline \hat{c} axis. The major features which appear between 3 and 8 MHz can be attributed to five quadrupole lines from distant Al nuclei,²³ and the $m = +\frac{1}{2}$ to $-\frac{1}{2}$ transition of distant Na ($I = \frac{3}{2}$, $g_{\text{Na}} = 1.015g_{\text{Al}}$). The distant Al quadrupole interaction displayed axial

symmetry as predicted by the crystal structure, and the data can be fit with a P_{\parallel}/h value of 0.39(7) MHz.

The broad, structureless ENDOR resonance which appears around 10 MHz in Fig. 7 is of greater interest since it represents a portion of the ENDOR signal expected from Na nuclei close to the F^+ center. The relative sizes of the hyperfine and nuclear-Zeeman interactions for these Na nuclei are such that one predicts two sets of quadrupole lines centered about $g_{\text{Na}}\mu_B H_0/h$ and split in frequency by the hf interaction A/h . We were unable to resolve the lower companion to the 10-MHz ENDOR line because of a spurious spectrometer response at frequencies below 2 MHz. The observed shift of the higher frequency Na ENDOR response with magnetic field orientation indicated that the direction of the Na color-center bond was perpendicular to the \hat{c} axis of the crystal. Averaging over the various bond directions within the conduction plane,²⁴ this hf interaction can be described approximately by

$$\vec{S} \cdot \underline{A}_{\text{Na}} \cdot \vec{I} = [a - (b/2)(3 \cos^2 \theta - 1)] S_z I_z, \quad (6)$$

with $a/h = 9.5(3)$ MHz, $b/h = 1.5(3)$ MHz, and θ represents the angle between the applied magnetic field and the crystalline \hat{c} axis. From the ENDOR data, it was not possible to resolve any Na quadrupole splittings, or to observe deviations from axial symmetry in the hf interaction. Figure 8 is the 3–13-MHz ENDOR spectrum of Na β -alumina

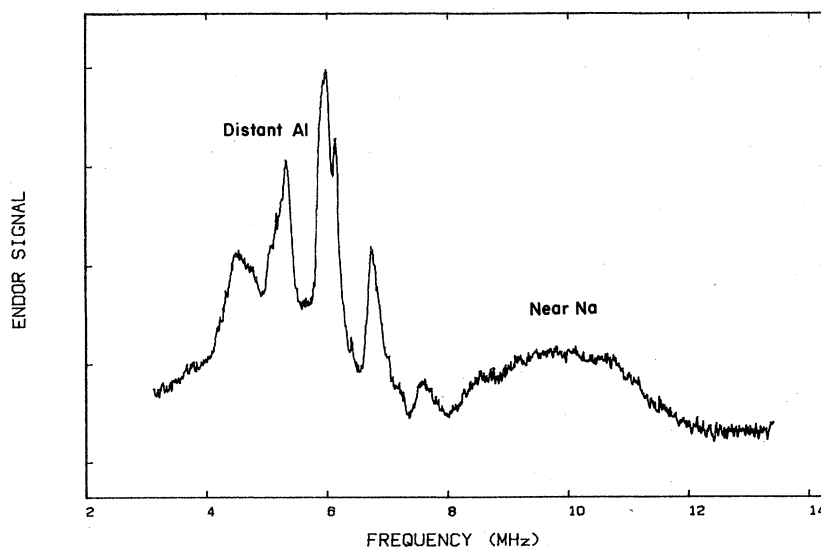


FIG. 7. Low-frequency ENDOR spectrum of Na β -alumina. $H_0 = 5346$ G, $\nu = 15.02$ GHz, and $\vec{H}_0 \parallel \hat{c}$. The broad near Na line is shown along with the distant Al spectrum.

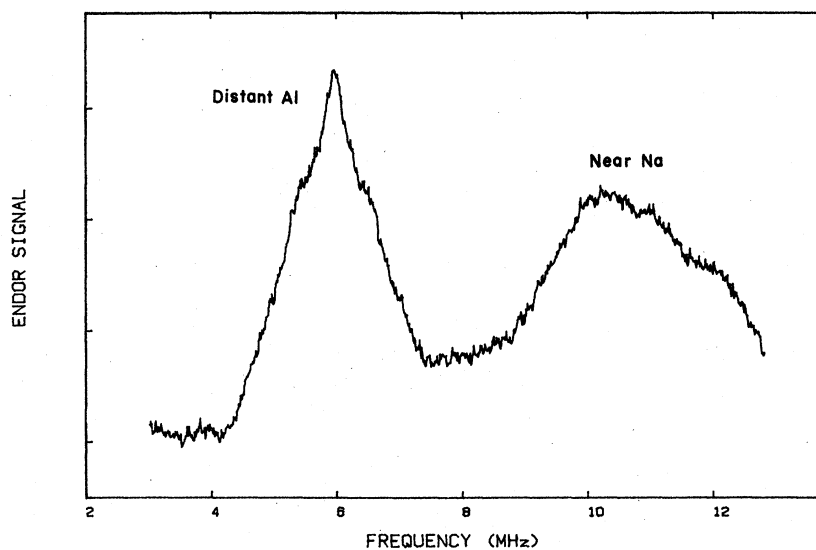


FIG. 8. Low-frequency ENDOR spectrum of Na β -alumina. $H_0=5346$ G, $\nu=15.02$ GHz, and $\vec{H}_0 \perp \hat{c}$.

with the external field of 5346 G oriented perpendicular to the crystalline \hat{c} axis.

Samples of Na β -alumina irradiated at low temperature with 0.75-MeV electrons contained the unidentified center but not the F^+ center. The EPR of this center was identical to that produced by γ irradiation as described in Sec. II. Figure 9 is the 3–25-MHz ENDOR spectrum of this center

with the external magnetic field parallel to the \hat{c} axis. A resonance due to distant Al was observed at $g_{Al}\mu_B H_0/h \approx 5.9$ MHz. In addition, five strong lines appear between 10 and 20 MHz, which we attribute to quadrupole splitting of near Al. In this case the spectrum should consist of two sets of five lines, centered at $g_{Al}\mu_B H_0/h$ and separated by $A_{||}/h$. The low-frequency set of resonances were

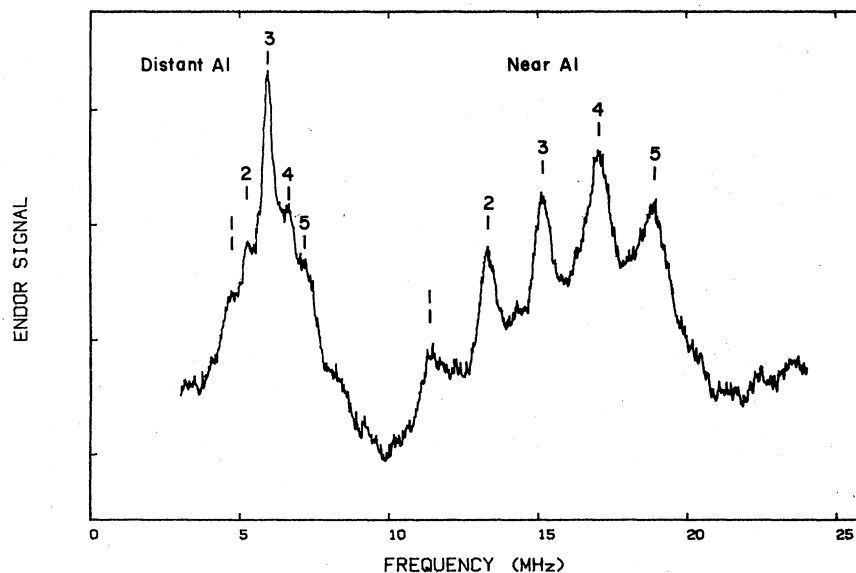


FIG. 9. ENDOR spectrum of the unidentified center in Na β -alumina with $H_0=5250$ G, $\nu=15.05$ GHz, and $\vec{H}_0 \parallel \hat{c}$. The distant Al lines are seen near 5.8 MHz. Five quadrupole lines from near Al are found between 10 and 20 MHz.

not observed because of experimental limitations. Using this interpretation we find $A_{||} = 18$ MHz, $A_{\perp} = 24$ MHz, and $P_{||} = 0.9$ MHz, in good agreement with the hyperfine splitting observed in the EPR spectrum of this center.

B. K β -alumina results

The EPR spectrum of the F^+ center in K β -alumina is similar to that obtained in Na β -alumina. Once more, the characteristic 11-line hyperfine splitting was observed, and there were only minor changes in g and A with $g_{||} = 2.0075(5)$, $g_{\perp} = 2.0043(5)$, $A_{||}/g_{||}\mu_B = 16.4$ G, and $A_{\perp}/g_{\perp}\mu_B = 15.5(2)$ G for K β -alumina. The most noticeable difference in the F^+ EPR data for the two materials was in the width of the hf lines. For $\vec{H}_0 || c$ in Na β -alumina, the linewidth ΔH was 11 G, but in K β -alumina the linewidth was only 5 G.⁸ This is consistent with the idea that the linewidth is due partially to the unresolved Na or K hf interactions⁶; the nuclear moment of ^{39}K being significantly smaller than that of ^{23}Na .

A near Al ENDOR spectrum is shown in Fig. 10. The two large ENDOR lines in this figure are associated with the hf splitting observed in the EPR data. A fit of the hf interaction for these resonances yields $a/h = 44.3(2)$ MHz and $b/h = 0.7(1)$ MHz in agreement with $A_{||}$ and A_{\perp} values from the EPR spectra. A second pair of ENDOR lines, denoted Al', in Fig. 10 are identi-

fied as an additional near Al resonance by the separation of the two lines, $2g_{\text{Al}}\mu_B H_0$. Features associated with the Al' ligand were not observed in the EPR spectra. The Al' hf interaction is highly isotropic with $a'/h = 34.7(7)$ MHz and $b'/h \leq 0.7$ MHz. Further discussion of the Al' ENDOR resonance will be resumed after presentation of data from Li β -alumina where a similar resonance is observed.

The K β -alumina ENDOR measurements on the F^+ center did not reveal any K resonance. The weak K hf interaction and small Zeeman energy causes the broad, near ^{39}K lines to overlap and occur at a low enough frequency to make these lines unresolvable. A distant Al resonance similar to the one in Na β -alumina was observed in K β -alumina with $P_{||} = 0.4(1)$ MHz.

C. Li β -alumina results

The irradiation and annealing procedure which produced the F^+ centers in Na and K β -alumina creates two varieties of F^+ centers in Li β -alumina. These centers are revealed by the Li β -alumina EPR spectrum shown in Fig. 11. This spectrum consists of a strong 11-line pattern with an intensity ratio indicative of two equivalent Al ligand nuclei. The center associated with the intense 11-line hyperfine splitting is denoted with a superscript prime. The weaker lines in this EPR spectrum are part of another 11-line hyperfine in-

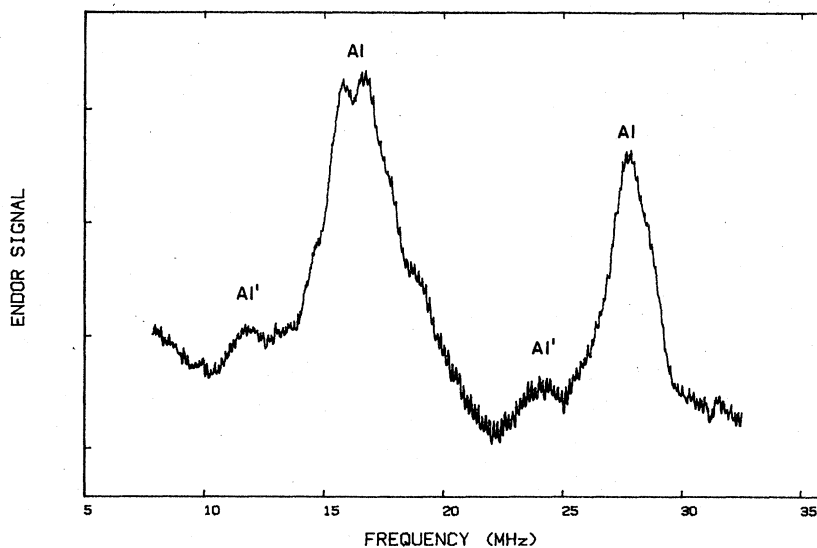


FIG. 10. ENDOR spectrum of near Al nuclei in K β -alumina. $H_0 = 5318$ G, $\nu = 14.96$ GHz, and $\vec{H}_0 || \hat{c}$. The Al and Al' resonances are indicated.

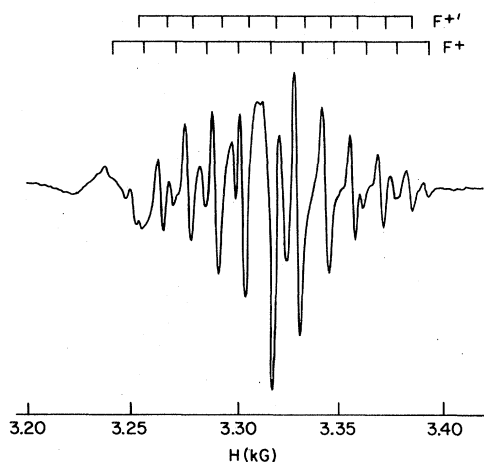


FIG. 11. Derivative of the EPR spectrum from F^+ centers in the conduction plane of Li β -alumina as measured at 77 K and 9.317 GHz, with $\vec{H}_0 \parallel \hat{c}$. Features of the eleven-line pattern displayed in Fig. 4 are still visible.

teraction belonging to a center denoted with no superscript.

The EPR spectra of both centers can be resolved by plotting the position of each hyperfine line for different \vec{H}_0 orientations as shown in Fig. 12. This figure clearly displays the two distinct 11-line patterns indicated by diamonds (primed center) and squares (unprimed center). The EPR spectrum for each center can be described by a hf tensor having axial symmetry along the \hat{c} axis. The solid lines in Fig. 12 result from a computer fit of the data and yield $g_{\parallel} = 2.0069(5)$, $g'_{\parallel} = 2.0059(5)$, $g_{\perp} = 2.0083(5)$, $g'_{\perp} = 2.0049(5)$, $A_{\parallel}/g_{\parallel}\mu_B = 13.2(2)$ G, $A'_{\parallel}/g'_{\parallel}\mu_B = 12.9(2)$ G, $A_{\perp}/g_{\perp}\mu_B = 15.2(2)$ G, and $A'_{\perp}/g'_{\perp}\mu_B = 14.5(2)$ G.

Analysis of the EPR spectra verifies that each of these color centers interacts with two equivalent Al nuclei. The symmetry of \underline{A} indicates that \hat{c} is the bond axis for the Al- F^+ -Al bond, and the spin-Hamiltonian parameters for this center closely resemble those obtained for the F^+ center in Na and K β -alumina. The weak anisotropy of the $F^{+'}$ center makes it more difficult to determine the direction of the Al- $F^{+'}$ -Al bond, and the strength of this hyperfine interaction is slightly reduced from the Al- F^+ coupling. These factors suggest that the small deviations in g and \underline{A} for these centers are probably caused by different environments within the conduction plane.

ENDOR measurements on near Al in Li β -alumina did not reveal much additional informa-

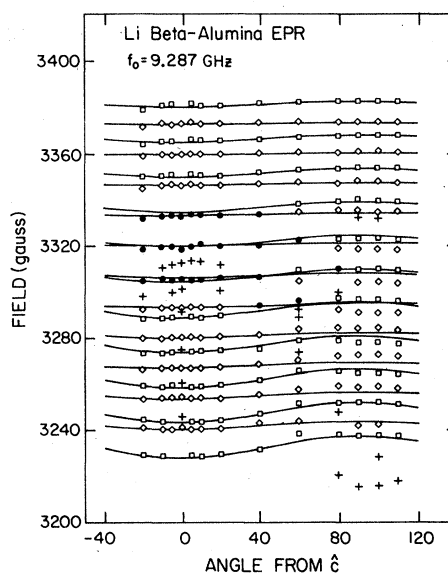


FIG. 12. Peak positions in the Li β -alumina EPR spectrum as a function of the applied magnetic field direction. Data indicated by diamonds produced the fit of the $F^{+'}$ center. Squares indicate data for the F^+ -center fit, and solid circles represent data used in the fit of both centers. The crosses were not used in either fit. The solid lines result from fits of both the F^+ and $F^{+'}$ centers to Eq. (4) of the text.

tion on the hf interactions of the two centers because the resonances were very broad. The data did confirm, however, that hf interactions due to Al ligands are present in the Li salt with isotropic components of $a/h \approx 42$ MHz and $a'/h \approx 36$ MHz. The near Al hf parameters of the prime center in Li β -alumina closely resemble those of the Al' center in K β -alumina. This suggests that the $F^{+'}$ center is present at low concentrations in the K salt as well.

The low-frequency ENDOR lines in Li β -alumina are displayed in Fig. 13. The near and distant Li lines are seen as a broad peak near $g_{Li}\mu_B H_0 = 8.9$ MHz. The model for the F^+ -center wave function predicts that the Fermi contact hyperfine interaction with the near ^7Li is ~ 2.0 MHz. For this reason, it is not possible to resolve the Li hyperfine interaction from the broad Li ENDOR line. A weak Li hyperfine coupling is confirmed by the Li β -alumina EPR linewidth which is comparable to that observed in K β -alumina. The distant Al spectrum at 6 MHz is very complex, but it is still possible to identify five major splittings with $P_{\parallel}/h = 0.43(6)$ MHz. The additional ENDOR

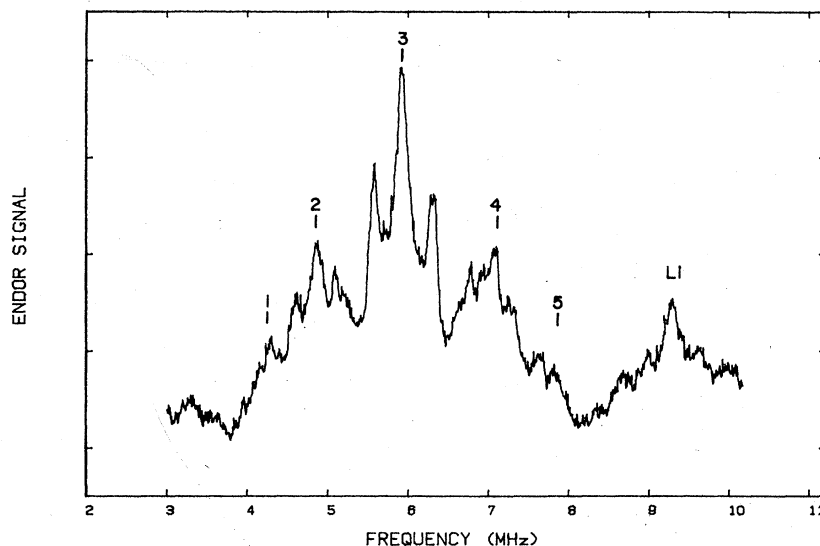


FIG. 13. Low-frequency ENDOR spectrum of Li β -alumina. $H_0 = 5346$ G, $\nu = 15.04$ GHz, and $\vec{H}_0 \parallel \hat{c}$. A five-line distant Al quadrupole structure is indicated, and a broad Li line is also shown.

lines probably result from the other distant Al nuclei or near Al nuclei with hyperfine couplings comparable to the size of the quadrupole splitting.

D. Discussion of the F^+ data

Until this point, no arguments have been given for identifying the color center as an F^+ center, but with all of the data presented, it is now possible to outline the identification process.⁶ All of the spin Hamiltonian parameters obtained from the EPR and ENDOR experiments are listed in Tables I–III. These tables provide a useful reference during this discussion, and for convenience all elements of \underline{A} have been converted to units of MHz.

The dominant characteristic, common to all the EPR data from these centers, is an 11-line hf pattern which has axial symmetry about the crystallographic \hat{c} axis and exhibits intensity ratios of 1:2:3:4:5:6:5:4:4:2:1. This indicates that the color center is equidistant from two Al nuclei and that the Al– F^+ –Al bond axes run parallel to the hexagonal \hat{c} axis. The only color-center locations with these properties lie in the mirror plane. The closest Al nuclei to this plane are found above and below the bridge oxygen sites or the charge-compensation oxygen sites.²⁵

In order to identify the type of color centers present in the conduction plane it is necessary to look closely at the magnitude of various spin Hamiltonian parameters. The fact that the g factors are

so close to the free-electron value suggests that the wave function of the color center is an s or p state. For a p -state color center, the g tensor displays axial symmetry along the axis of the p lobe containing the unpaired spin, and there is significant g -factor anisotropy with $g_{\parallel} \approx g_e$ and $g_{\perp} - g_e = 0.1 - 0.01$.^{19,26} The EPR data show that there is a significant deviation from g_e when \vec{H}_0 is parallel to the \hat{c} axis. This would place the p lobe in the conduction plane and produce a small contact interaction with the Al nuclei above and below the conduction plane. This contradicts the data which exhibit a large aluminum contact interaction. Also, the g -factor shift from g_e is much smaller than the shift normally observed for a p -state color center. For these reasons p -state centers such as the O^- center are rejected as a plausible explanation for this color center in β -alumina.

The observed g -factor shifts and Al contact hyperfine interactions suggest instead that the color center is an s -state defect. The model for such a defect is an electron trapped at a conduction-plane O^{2-} vacancy (see Fig. 3). This color center is commonly called an F^+ center because a local positive charge remains due to the absence of the divalent oxygen ion. To a first approximation, the F^+ center, like the F center, has a hydrogenic s -state wave function. The F -center g shift is produced by the electron spin-orbit interaction with neighboring nuclei, and this model predicts $g - g_e \leq 0$ in agreement with the data for F centers

TABLE I. F^+ spin Hamiltonian parameters for Na β -alumina obtained from EPR and ENDOR measurements. The results of other independent studies are included for comparison.

Parameter	Units	Expt. value	Source	Ligand
g_{\parallel}	...	2.0079(5)	This EPR	...
		2.0076(2)	a	
		2.0085	b	
		2.0039(5)	This EPR	
g_{\perp}	...	2.0036(2)	a	...
		2.0049	b	
		47.2(6)	This EPR	
A_{\parallel}/h	MHz	46.78(6)	a	Al
		47.0	b	
		45.7(6)	This EPR	
A_{\perp}/h	MHz	45.35(8)	a	Al
		45.2	b	
		45.7(1)	This ENDOR	
a/h	MHz	45.20(7)	c	Al
b/h	MHz	1.0(1)	This ENDOR	Al
		1.20(2)	c	
P_{\parallel}/h	MHz	0.35(6)	This ENDOR	Al
		0.383(7)	d	
a/h	MHz	9.5(3)	This ENDOR	Na
		7.8(2)	c	
b/h	MHz	1.5(3)	This ENDOR	Na
		1.2(2)	c	
P_{\parallel}/h	MHz	0.7(1)	c	Na
P_{\perp}/h	MHz	0.39(7)	This ENDOR	Distant Al

^aReference 6.

^bReference 8.

^cReference 21.

^dReference 22.

in alkali halides.²⁷ However, in oxides and other divalent materials $g - g_e > 0$ has frequently been observed for F^+ centers with g shifts similar to those observed in β -alumina.²⁸ This effect has been attributed to the admixture of a charge-transfer state where a hole is trapped at a neighboring anion.²⁹ Using this model it is possible to suggest that a neighboring oxygen within the conduction plane interacts with the F^+ center producing the

size and asymmetry of the g shifts, but this calculation has not been attempted.

The magnitude of the observed hyperfine interactions is in agreement with those expected for an F^+ center. The O-Al distance at the bridge oxygen is 1.68 Å with $a/g_{Al}h = 31$ MHz from Al ENDOR data on Na β -alumina. By comparison, the F^+ center in MgO displays a contact interaction with ²⁵Mg such that $a/g_{Mg}h = 32$ MHz, where the

TABLE II. F^+ spin Hamiltonian parameters for K β -alumina obtained from EPR and ENDOR measurements. The results of another independent study are included for comparison.

Parameter	Units	Expt. Value	Source	Ligand
g_{\parallel}	...	2.0075(5)	This EPR	...
		2.0076	a	
g_{\perp}	...	2.0043(5)	This EPR	...
		2.0049	a	
A_{\parallel}/h	MHz	46.0(6)	This EPR	Al
		46.4	a	
A_{\perp}/h	MHz	43.5(6)	This EPR	Al
		44.3	a	
a/h	MHz	44.3(2)	This ENDOR	Al
b/h	MHz	0.7(1)	This ENDOR	Al
a'/h	MHz	34.7(7)	This ENDOR	Al'
b'/h	MHz	≤ 0.7	This ENDOR	Al'
P_{\parallel}/h	MHz	0.4(1)	This ENDOR	Distant Al

^aReference 8.

Mg-O distance is 2.1 Å.³⁰ The magnitude of the near Al dipolar interaction is

$$\frac{b_{Al}}{h} \sim \frac{g_{Al}g_{\mu_B}^2}{hR_0^3} = 4.36 \quad (7)$$

expressed in MHz, where $R_0 = 1.68$ Å. This classically estimated dipolar hf parameter is about four

times that observed for Al in Na β -alumina. The same corrections to the electronic wave function that explain the g -factor shifts also produce deviations in the dipolar coupling.^{6,31}

The measured quadrupole couplings are also consistent with other data. The quadrupole interaction for the near Al resonance has the expected

TABLE III. F^+ spin Hamiltonian parameters for Li β -alumina obtained from EPR and ENDOR measurements.

Parameter	Units	Expt. value	Source (this work)	Ligand
g'_{\parallel}	...	2.0069(5)	EPR	...
g'_{\perp}	...	2.0059(5)	EPR	...
g_{\parallel}	...	2.0083(5)	EPR	...
		2.0049(5)	EPR	
A'_{\parallel}/h	MHz	37.0(6)	EPR	Al'
A'_{\perp}/h	MHz	36.3(6)	EPR	Al'
A_{\parallel}/h	MHz	42.6(6)	EPR	Al
A_{\perp}/h	MHz	40.6(6)	EPR	Al
a'/h	MHz	~ 36	ENDOR	Al'
a/h	MHz	~ 42	ENDOR	Al
P_{\parallel}/h	MHz	0.43(6)	ENDOR	Distant Al

symmetry axis for an adjacent F^+ center located along the \hat{c} axis, and calculations indicate that the quadrupole splitting is due largely to the electric field gradient produced by the effective positive point charge of the F^+ center.²¹ The resolved distant Al quadrupole splitting, $P_{||}/h \approx 0.4$ MHz, is the same as the largest Al quadrupole coupling observed in NMR measurements.³²

Based on this discussion, it is possible to conclude that the 11-line EPR spectrum is caused by an F^+ center located at a conduction plane oxygen site. The observed g factors and hyperfine interactions are all in agreement with this model, and as a result of the EPR and ENDOR experiments, enough is known about the conduction plane color centers to allow a quantitative confirmation of the model proposed by Kurtz and Stapleton¹⁰ to explain the anomalous spin relaxation of F^+ centers in Na, K, and Li β -alumina.

Although poor resolution of the near cation ENDOR data makes it difficult to learn specific details about the disorder in the conduction plane, some insight can be gained by simulating the experimental Na ENDOR lineshapes which appear in Figs. 7 and 8. The width of the Na ENDOR line with $\vec{H}_0 \perp \hat{c}$ could be due to the overlap of signals from Na ions in the different Beever-Ross (BR) sites. These sites are inequivalent for an arbitrary angle of the magnetic field in the plane and would result in three lines. However, with $\vec{H}_0 \parallel \hat{c}$, these

sites are equivalent and should give rise to one, relatively sharp resonance line. This is not observed. Instead, we simulate these lines assuming that the width is due to Gaussian distributions of the hf and quadrupole interactions of the ligand nuclei. We consider only nearest-neighbor BR and mid-oxygen (MO) sites to make significant contributions to the Na ENDOR lineshape. This is because the anti-Beevers-Ross (aBR) site has a low probability of occupancy and because we assume that both the contact and dipolar hf interactions scale with distance as R^{-3} . The BR, MO, and aBR sites are shown schematically in Fig. 2 and are situated 3.23, 2.80, and 3.23 Å from a conduction plane oxygen, respectively.

Using site occupancy probabilities of 0.63 and 0.36 for the BR and MO sites, the average contribution to the ENDOR signal from MO sites is 57% of that from BR sites. With this relative intensity we do a four-parameter ENDOR lineshape simulation using A_{BR} , the mean hf coupling constant for the BR site; ΔA , the standard deviation of the hf coupling at both the BR and MO sites; $P_{||}$, the quadrupole coupling; and $\Delta P_{||}$, the corresponding standard deviation. Since $|\psi(0)|^2$ at a ligand nucleus scales roughly as $Z^{1.5}/R^3$ for an F center with a ligand of atomic number Z ,^{33,34} we can estimate the contact and dipolar hf couplings of ligand nuclei at the MO site from the corresponding values at the BR site. Thus, once A_{BR} is chosen,

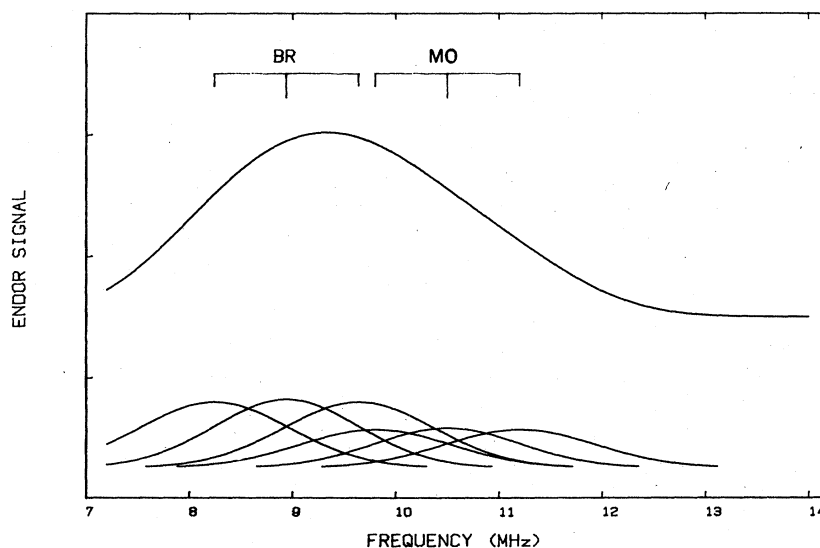


FIG. 14. Simulation of the near Na ENDOR resonance in Na β -alumina for $\vec{H}_0 \parallel \hat{c}$. In the lower portion of the figure the resonance is decomposed into its constituent parts: three inhomogeneously broadened quadrupole resonances from BR sites, and three similar resonances from MO sites. The values of the parameters are given in the text. This simulation should be compared to the experimental data of Fig. 7.

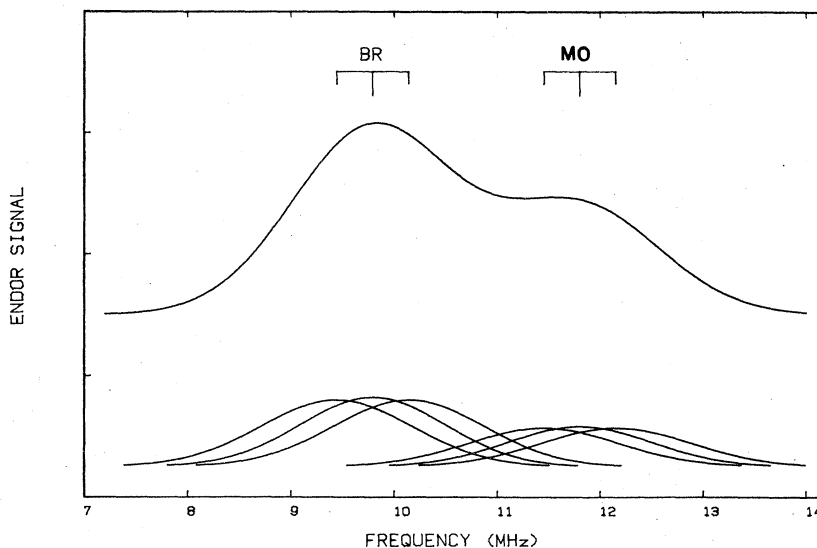


FIG. 15. Simulation of the near Na ENDOR resonance in Na β -alumina for $\vec{H}_0 \perp \hat{c}$. In the lower portion of the figure the resonance is decomposed into its constituent parts: three inhomogeneously broadened quadrupole resonances from BR sites, and three similar resonances from MO sites. The values of the parameters are given in the text. This simulation should be compared to the experimental data of Fig. 8.

A_{MO} follows from scaling. The same averaging procedure used to determine the angular dependence of A_{Na} [Eq. (6)] yields a quadrupole shift of $-P_{||}(3 \cos^2 \theta - 1)(2m + 1)/4$. It is obvious that $\Delta P_{||}$ alone cannot account for the large ENDOR linewidth since the $m = \frac{1}{2}$ to $-\frac{1}{2}$ nuclear transitions are unaffected by quadrupole interactions and would produce sharp lines.

Figure 14 is a simulation of the ENDOR lineshape for $\vec{H}_0 \parallel \hat{c}$ and should be compared to Fig. 7. Similarly Fig. 15 corresponds to $\vec{H}_0 \perp \hat{c}$ and should be contrasted with Fig. 8. These simulations reproduce the position, shape, and angular dependence of the near Na resonance and correspond to $a/h = 7.0$ MHz and $b/h = 1.1$ MHz for the BR site. The corresponding values at the MO site are 10.7 and 1.7 MHz. These simulation parameters should be compared with the experimental data of Table I, where no distinction with respect to sites is possible. The values of ΔA , $P_{||}$, and $\Delta P_{||}$ used in the simulations were 0.7, 0.7, and 0.2 MHz, respectively. $P_{||}$ was chosen equal to that estimated by Barklie *et al.*²¹ Based upon the measured near Al contact interaction, our scaling procedure predicts $a/h = 5.2$ MHz for the Na ions at the BR site. This value is within 25% of that used in the simulations. Assuming the simulation value for the contact hf coupling of 7.0 MHz for

Na at the BR site, the $Z^{1.5}$ scaling predicts contact hf couplings of only 1.5 and 2.8 MHz for Li and K ligands, respectively. These small contact terms make resolution of the K and Li hf interactions impossible from the ENDOR data.

The width of the nearby, mobile cation ENDOR resonance may be related to the existence of localized tunneling states. These states have been used to explain the low-temperature thermal and dielectric properties of Na β -alumina.¹⁻⁴ The dielectric susceptibility data on Na β -alumina can be understood by assuming that the Na ions tunnel in the conduction plane between the minima of two potential wells, about 0.3 Å apart. With a $1/R^3$ scaling of the hf coupling, this corresponds to a 28% variation in $A_{||}$ at the BR site in Na β -alumina if the tunneling were in the conduction plane along a radial from the F^+ center. A value of 12% for $\Delta A_{||}/A_{||}$ was used in our simulation.

Such a mechanism cannot account for the excessive width of the near Al ENDOR lines. An alternative explanation is that the different local environments, caused either by disorder in cation locations, or by tunneling, modify the F^+ -center wave function. This could change the Fermi contact hf term with both the Na and Al ligands, causing inhomogeneously broadened nuclear energy levels. A similar mechanism may be responsible

for the existence of the $F^{+'}$ center in Li β -alumina. The observed shifts in both the g factors and the anisotropic hf parameter relative to the F^+ center, are consistent with a change in the p character in the F^+ wave function.³¹ There is evidence that the Li ions may move 0.85 Å perpendicular to the mirror plane.^{3,35} This additional degree of freedom for the disorder may be responsible for the clear resolution of the $F^{+'}$ center in the EPR spectrum of the Li salt.

V. CONCLUSIONS

These Ku-band ENDOR measurements have confirmed independent x -band ENDOR data on F^+ centers in Na β -alumina and have extended the measurements to include K and Li β -alumina. Evidence of additional, closely related centers in

the Li and K salt has been presented. We have correlated the broad Na ENDOR linewidth with disorder and tunneling distances in the conduction plane of Na β -alumina as measured from the dielectric susceptibility data of others.

ACKNOWLEDGMENTS

One of us (H.J.S.) wishes to acknowledge the cooperation of the Solid State Division of the Oak Ridge National Laboratory while he was a visitor on sabbatical leave during which preliminary aspects of this work were begun. This research was supported in part by the U.S. Department of Energy under Contract No. DE-AC02-76ER01198. Oak Ridge National Laboratory is operated by Union Carbide Corporation for the U.S. Department of Energy under Contract No. W-7405-ENG-26.

*Present address: Sandia Laboratories, Albuquerque, N.M. 87185.

¹P. J. Anthony and A. C. Anderson, Phys. Rev. B **14**, 5198 (1976).

²P. J. Anthony and A. C. Anderson, Phys. Rev. B **16**, 3827 (1977).

³P. J. Anthony and A. C. Anderson, Phys. Rev. B **19**, 5310 (1979).

⁴U. Strom, M. von Schickfus, and S. Hunklinger, Phys. Rev. Lett. **41**, 910 (1978).

⁵J. H. Kennedy, in *Topics in Applied Physics*, edited by S. Geller (Springer-Verlag, New York, 1977), Vol. 21, Chap. 5, and references therein. The effects of this disorder are more easily studied in β -alumina than in other amorphous materials since the disorder is confined to the mirror planes.

⁶K. O'Donnell, R. C. Barklie, and B. Henderson, J. Phys. C **11**, 3871 (1978).

⁷S. R. Kurtz and H. J. Stapleton, Phys. Rev. Lett. **42**, 1773 (1979).

⁸D. Gourier, D. Vivien, and J. Livage, Phys. Status Solidi A **56**, 247 (1979).

⁹S. R. Kurtz and H. J. Stapleton, in *Fast Ion Transport in Solids*, edited by P. Vashishta, J. N. Mundy, and G. K. Shenoy (North-Holland, Amsterdam, 1979).

¹⁰S. R. Kurtz and H. J. Stapleton, Phys. Rev. B **22**, 2195 (1980).

¹¹P. J. Anthony, Ph.D. thesis, University of Illinois at Urbana-Champaign, 1978 (unpublished).

¹²R. C. Barklie and K. O'Donnell, J. Phys. C **10**, 4127 (1977).

¹³D. Gourier, J. Antoine, D. Vivien, J. Thery, J. Livage, and R. Collongues, Phys. Status Solidi A **41**, 423 (1977).

¹⁴J. Antoine, D. Vivien, J. Thery, and R. Collongues, J. Solid State Chem. **21**, 349 (1977).

¹⁵Manufactured by Emerson and Cuming, Inc., Canton, Mass.

¹⁶Manufactured by Precision Tube Co., North Wales, Pa.

¹⁷M. Giordana, F. Momo, and A. Stogiu, J. Phys. E **12**, 815 (1979).

¹⁸A. Abragam and B. Bleaney, *Electron Paramagnetic Resonance of Transition Metal Ions* (Clarendon, Oxford, 1970).

¹⁹B. Henderson and J. E. Wertz, *Defects in the Alkaline Earth Oxides* (Taylor and Francis, London, 1977).

²⁰R. C. Barklie, J. R. Niklas, and J. M. Spaeth, J. Phys. (Paris) **41**, C6-537 (1980).

²¹R. C. Barklie, J. R. Niklas, and J. M. Spaeth, J. Phys. C **13**, 1745 (1980).

²²R. C. Barklie, J. R. Niklas, and J. M. Spaeth, J. Phys. C **13**, 1757 (1980).

²³J. Lambe, N. Laurance, E. C. McIrvine, and R. W. Terhune, Phys. Rev. **122**, 1161 (1961).

²⁴Equation (6) is obtained by rotating each of the three hf tensors into the crystal coordinate system, and averaging over the sum. Identical results were obtained in Ref. 21.

²⁵W. L. Roth, J. Solid State Chem. **4**, 60 (1972); W. L. Roth, F. Reidinger, and S. LaPlaca, in *Superionic Conductors*, edited by Gerald D. Mahan and Walter

- L. Roth (Plenum, New York, 1977).
- ²⁶O. F. Schirmer, *J. Phys. Chem. Solids* 32, 499 (1971).
- ²⁷Jordan J. Markham, in *Solid State Physics*, edited by Frederick Seitz and David Turnbull (Academic, New York, 1966), Suppl. 8.
- ²⁸J. E. Wertz, J. W. Orton, and P. Auzins, *Discuss. Faraday Soc.* 31, 140 (1961).
- ²⁹R. H. Bartram, C. E. Swenberg, and S. Y. La, *Phys. Rev.* 162, 759 (1967).
- ³⁰W. P. Unruh and J. W. Culvahouse, *Phys. Rev.* 154, 861 (1967).
- ³¹H. Seidel and H. C. Wolf, in *Physics of Color Centers*, edited by W. Beall Fowler (Academic, New York, 1968), p. 557.
- ³²Intaik Chung, Ph.D. thesis (State University of New York at Albany, 1974) (unpublished).
- ³³A. E. Hughes and B. Henderson, in *Point Defects in Solids*, edited by J. H. Crawford and L. M. Slifkin (Plenum, New York, 1972), Vol. 1.
- ³⁴W. C. Holton and H. Blum, *Phys. Rev.* 129, 89 (1962).
- ³⁵J. C. Wang, J. B. Bates, and T. Kaneda, *Bull. Am. Phys. Soc.* 23, 241 (1978).